Insight derived from molecular docking and molecular dynamics simulations into the binding interactions between HIV-1 protease inhibitors and SARS-CoV-2 3CLpro

Peng Sang [1] , Shu-Hui Tian [1] , Zhao-Hui Meng [2,*], Li-Quan Yang [1,*]

1 College of Agriculture and Biological Science, Dali University, Dali, P. R. China;
2 Laboratory of Molecular Cardiology, Department of Cardiology, The First Affiliated Hospital of Kunming Medical University, Kunming, P. R. China.
* Author to whom correspondence should be addressed: E-Mail: speng431@163.com, ylqbioinfo@gmail.com.

Abstract: A novel severe acute respiratory syndrome coronavirus (SARS-CoV-2) was identified from respiratory illness patients in Wuhan, Hubei Province, China, which has recently emerged as a serious threat to the world public health. Hower, no approved drugs have been found to effectively inhibit the virus. Since it has been reported that the HIV-1 protease inhibitors can be used as anti-SARS drugs by tegarting SARS-CoV 3CLpro, we choose six approved anti-HIV-1 drugs to investigate their binding interactions between 3CLpro, and to evaluate their potential to become clinical drugs for the new coronavirus pneumonia (COVID-19) caused by SARS-CoV-2 infection. The molecular docking results indicate that, the 3CLpro of SARS-CoV-2 has a higher binding affinity for all the studied inhibitors than its SARS homologue. Two docking complexes (indinavir and darunavir) with high docking scores were futher subjected to MM-PBSA binding free energy calculations to detail the molecular interactions between these two proteinase inhibitors and the 3CLpro. Our results show that darunavir has the best binding affinity with SARS-CoV-2 and SARS-CoV 3CLpro among all inhibitors, indicating it has the potential to become an anti-COVID-19 clinical drug. The likely reason behind the increased binding affinity of HIV-1 protease inhibitors toward SARS-CoV-2 3CLpro than that of SARS-CoV were investigated by MD simulations. Our study provides insight into the possible role of structural flexibility during interactions between 3CLpro and inhibitors, and sheds light on the structure-based design of anti-COVID-19 drugs targeting the SARS-CoV-2 3CLpro.

Keywords: SARS-CoV-2; HIV-1 protease inhibitors; darunavir; molecular docking; binding free energy

1. Introduction

From December 2019, an outbreak of new coronavirus pneumonia (named COVID-19 by WHO) caused by a novel coronavirus (named SARS-CoV-2 by ICTV) has become serious threat to the global health, resulting in 2791 deaths from 78959 cases as of 28 Feburary 2020 from China. SARS-CoV-2 has been identified as the seventh member of the family of coronaviruses [1]. Through the whole genome sequence alignment analysis, SARS-CoV-2 was found to have higher sequence homology toward SARS-CoV than that of MERS-CoV [2].

The coronaviruse geneome encodes four structural proteins: spike glycoprotein (S), small envelope protein (E), matrix glycoprotein (M) and nucleocapsid protein (N) [3]. In addition to

the above four structural genes, the 3CLpro, a main protease required for the maturation of coronaviruses, is vital for the viral life cycle, making it an attractive target of anti-coronavirus drug development [4, 5]. By sequence alignment, it is found that SARS-CoV-2 and SARS-CoV 3CLpro share remarkable 96% sequence identity (Fig. 1A). The crytal structure of SARS-CoV-2 3CLpro (PDB ID: 6LU7) is highly similar to its SARS sister (PDB ID: 1UJ1) [6], the backbone root mean square deviatio (RMSD) value between these two proteins is only 1.4 Å (Fig. 1C). Both of SARS-CoV-2 and SARS-CoV 3CLpro protomers contain nine α-helices and 13 β-strands that make up three distinct domains, i.e. domain I, domain II and domain III (Fig. 1B) [7, 8] . Similar to other CoV proteases, Domains I (residues 8–101) and II (residues 102–184) contain one antiparallel β-barrel, which resemble the trypsin-like serine proteases structure. Domain III (residues 201–306) consists of 5 α-helices (α5-α9), which are connected by a long loop (residues185–200) with domain II. In contrast to the common Ser–His–Asp catalytic triad of serine proteases, the SARS-CoV-2 and SARS-CoV 3CLpro has a catalytic dyad, which are composed of the conserved residues H41 and C145. The main substrate-binding site of the 3CLpro is formed by a cleft between domains I and II (Fig. 1B).

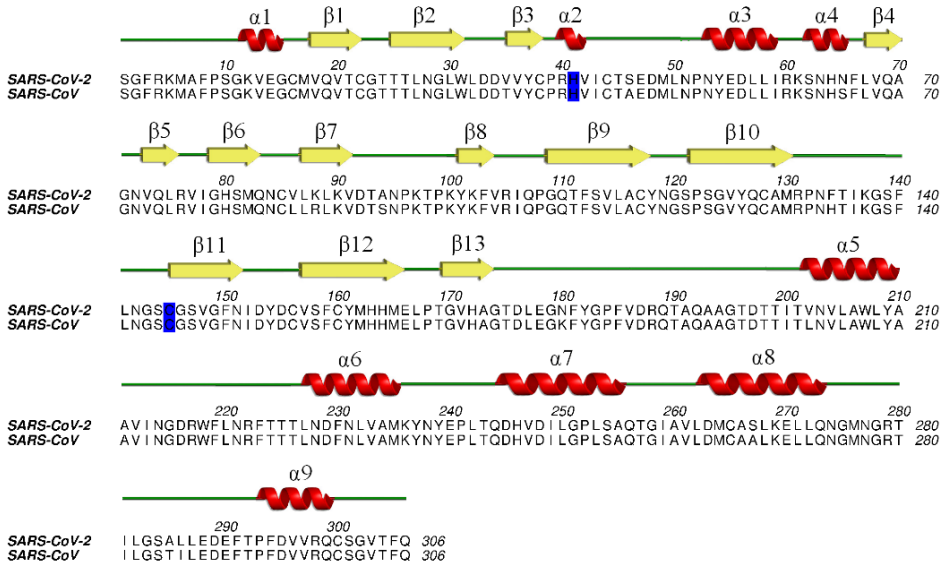

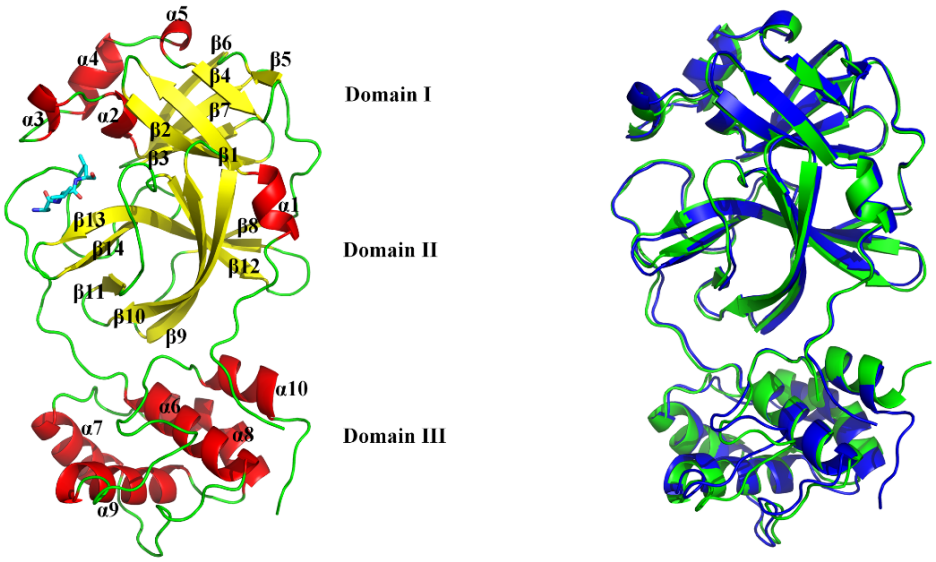

Fig. 1. Sequence alignment and 3D structure of SARS-CoV-2 and SARS-CoV 3CLpro. (A) Sequence alignment and secondary structures of SARS-CoV-2 and SARS-CoV 3CLpro. The secondary structures are illustrated above the corresponding amino acid sequence (red helix: α-helix, yellow arrow: β-sheet), and the residue numbers are indicated above the primary sequence. The H41 and C145 residues consisting the catalytic dyad are highlighted in blue. (A) was generated using Aline [9]. (B) Ribbon representation of SARS-CoV-2 (PDB code: 6LU7). The structural elements are indicated by color, where α-helices are red, β-sheets are yellow and loops are green, and the peptide-like inhibitor N3 is represented as a blue sphere. The catalytic dyad residues H41 and C145 are shown as magenta stick models. (C) Superimposed 3D structures of SARS-CoV-2 (PDB code: 6LU7, blue) and SARS-CoV (PDB code: 1UJ1, green) 3CLpro. (B) and (C) were generated using Pymol [10].

Although the SARS-CoV-2 3CLpro 3D structure provides deep insight into viral life cycle and facilitate for screening anti-COVID-19 drugs, no approved drugs have been found to effectively inhibit the virus so far. Since the emergency of this outbreak and it has been reported that the HIV-1 protease inhibitors can be used as anti-SARS drugs by tegarting SARS-CoV 3CLpro [11-13], we choose six public anti-HIV-1 drugs to evaluate their potential to become clinical drugs for COVID-19 by means of molecular docking. Two of the six drug-3CLpro complexes (indinavir and darunavir) showing high docking scores were futher subjected to molecular dynamics (MD) simulation and molecular mechanics Poisson-Boltzmann surface area (MM-PBSA) binding free energy calculations. The molecular interactions between these two HIV-1 proteinase inhibitors and the 3CLpro were detailed analyzed, and the reason for the difference of binding ability between SARS-CoV-2 and SARS-CoV 3CLpro and these inhibitors was also discussed.

2. Materials and methods

2.1 Preparation of the 3CLpro structure and HIV-1 protease inhibitors

The crystal structures of SARS-CoV-2 (PDB code: 6LU7) and SARS-CoV (PDB code: 1UJ1) 3CLpro were obtained from the Protein Data Bank (www.pdb.org), and any heteroatoms and water molecules were removed for molecular docking studies. Six HIV-1 protease-inhibitor complex structures were downloaded from the Protein Data Bank (PDB codes: 1MUI (lopinavir), 2B60 (ritonavir), 2BPX (indinavir), 3OXC (saquinavir), 4LL3(darunavir), 6DIF (tipranavir)), and the corresponding inhibitor (Fig. 2) was used for docking to the SARS-CoV-2 and SARS-CoV 3CLpro.

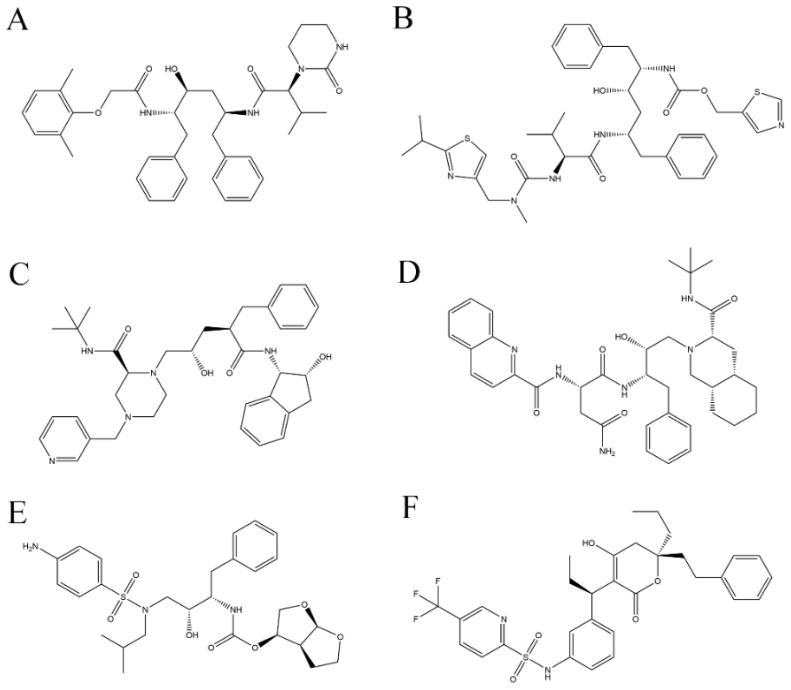

Fig. 2. Chemical structures of HIV-1 protease inhibitors used in this study. (A) lopinavir ($C_{37}H_{48}N_4O_5$). (B) ritonavir ($C_{37}H_{48}N_6O_5S_2$). (C) indinavir ($C_{36}H_{47}N_5O_4$). (D) saquinavir ($C_{38}H_{50}N_6O_5$). (E) darunavir ($C_{27}H_{37}N_3O_7S$). (F) tipranavir ($C_{31}H_{33}F_3N_2O_5S$).

2.2 Molecular Docking

To evaluate the binding affinity of these HIV-1 protease inhibitors and the 3CLpro, the comparative molecular docking analysis was carried out using Autodock 4.2 [14]. In docking simulation, the grid box was defined according the peptide-like inhibitor binding pocket of SARS-CoV-2 3CLpro（Fig. 3）. The size of affinity map were set at 40 Å× 50 Å× 40 Å, and spacing between the grid points was set to 0.375 Å. Docking was performed with Lamarckian genetic algorithm and default parameters. The best docked conformations (3CLpro-inhibitor complexes) with lowest docking energy were selected for further MD simulations and MM-PBSA binding free energy calculations.

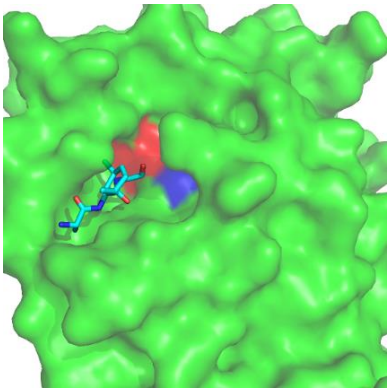

Fig. 3. Binding pocket of SARS-CoV-2 3CLpro (PDB code: 6LU7). Structure of 3CLpro is shown as molecular surface model in green. The peptide-like inhibitor is represented as stick model. The H41 and C145 residues consisting the catalytic dyad are highlighted in red and blue, respectively.

2.3 MD simulation

In order to explore the molecular interactions between HIV-1 proteinase inhibitors and the 3CLpro as well as the reason behind the difference of binding ability between SARS-CoV-2 and SARS-CoV 3CLpro and these inhibitors, four kinds of MD simulations were performed: SARS-CoV-2 3CLpro free enzyme (free SARS-CoV-2), SARS-CoV 3CLpro free enzyme (free SARS-CoV), SARS-CoV-2 3CLpro-inhibitor complex (SARS-CoV-2-inhibitor) and SARS-CoV 3CLpro-inhibitor complex (SARS-CoV-inhibitor). All the simulation were carried out using the GROMACS-5.1.4 software package [15] with the CHARMM36 all-atom force field (March, 2019) [16]. The force field of all the HIV-1 proteinase inhibitors was generated by the CGenFF server [17, 18].

Each simulation system was dissolved using TIP3P water model [19] and centered in a dodecahedron box with a 1.0 nm minimum distance between the protein and the edge of the box. The steepest descent algorithm was used to minimize the simulation enenrgy. The systems were equilibrated by two continuous 500-ps position restraint simulations of 1000kJ/mol/nm^2 in the NVT and NPT ensembles. All the equilibrated systems were then subjected to production MD runs. Other simulation parameters and conditions were the same as Ref [20].

2.4 Binding free energy calculation

The MM-PBSA method was used to compute the binding free energy of 3CLpro-inhibitor complexes during simulation. A detailed description of the MM-PBSA method is presented in Ref [21]. In this study, the binding free energy of the 3CLpro to HIV-1 proteinase inhibitors were calculated using the GROMACS tool g_mmpbsa [22]. When using MM-PBSA, the binding free energy of the protein and ligand was defined as

$$\Delta G_{binding} = \Delta G_{complex} - (\Delta G_{protein} + \Delta G_{ligand})$$

For each subunit, the free energy, G, can be presented as

$$G = E_{MM} + G_{sol} - TS$$

where E_{MM} represents the average molecular mechanical potential energy in vacuum, which includes electrostatic (E_{elec}) and van der Waals (E_{vdw}) interactions components and interprets them as

$$E_{MM} = E_{ele} + E_{vdw}$$

G_{sol} represents the solvation free energy which includes both electrostatic (G_{polar}) and non-electrostatic ($G_{nonpolar}$) components and interprets them as

$$G_{sol} = G_{polar} + G_{nonpolar}$$

Since the contribution of the entropic term (TS) is negligible when the computing models are very similar [11] and calculating the contribution of entropy to the binding free energy is challenging and time-consuming, the contribution of the entropic term was excluded in current

version of g_mmpbsa.

3. Results and discussion

3.1 Molecular docking of HIV-1 proteinase inhibitors against 3CLpro

We choose six approved anti-HIV-1 inhibitors to evaluate their potential to become clinical drugs for COVID-19. As shown in Table 1, the 3CLpro of SARS-CoV-2 has a lower binding energy for all the studied inhibitors than its SARS homologue, although both of their binding energy are higher than all the HIV-1 proteinase-inhibitor complexes served as positive control, indicating the binding affinity of SARS-CoV-2 3CLpro towards inhibitors are higher than that of SARS-CoV 3CLpro. Of the six HIV-1 proteinase inhibitors, indinavir and darunavir have been proved to have better binding affinity with SARS-CoV-2 3CLpro, and their binding energy values are close to HIV-1 proteinase. When comparing with each other, the binding energy of 3CLpro-darunavir complex (-10.24 kJ/mol) is lower than the 3CLpro-indinavir counterpart (-10.02 kJ/mol), indicating the binding affinity of darrunavir towards SARS-CoV-2 3CLpro might be higher than indinavir. Since 3CLpro is essential for coronaviral replication [7], the better inhibitory effect of these two inhibitors on the SARS-CoV-2 3CLpro can show that they have the potential to become anti-COVID-19 clinical drugs.

Table 1. Molecular docking analyses of six inhibitors towards 3CLpro and HIV-1 proteinase

Inhibitor	Binding energy (kJ/mol)		
	SARS-CoV-2	SARS-CoV	HIV-1 proteinase
lopinavir	-5.49	-2.12	-5.78
ritonavir	-2.34	-1.42	-5.17
indinavir	-10.02	-7.49	-11.56
saquinavir	-8.26	-5.3	-11.82
darunavir	-10.24	-7.5	-10.85
tipranavir	-5.8	-4.4	-11.07

The binding modes of indinavir and darunavir in their docking complexes are shown in Fig. 3. For the SARS-CoV-2 3CLpro（Fig. 4 A and B）, the binding pocket are in a more closed state, and indinavir and darunavir bind deeper into the pocket both with 19 contact residues. In contrast, the SARS-CoV 3CLpro binding pocket is in a more open state（Fig. 4 C and D）, and there are only 11 and 17 contact residues in 3CLpro-indinavir and 3CLpro-darunavir complexes, respectively. The more contact residues likely strengthen the binding affinity between SARS-CoV-2 3CLpro and inhibitors, which can explain why the binding energy values between them are lower than that of SARS-CoV 3CLpro-inhibitor complexes. Of note is that darunavir forms 5 and 3 hydrogen bonds with SARS-CoV-2 and SARS-CoV 3CLpro, respectively. By contrast, there is no hydrogen bond between indinavir and both of these two

3CLpro. Since the hydrogen bond plays an important role in the stability of the enzyme-inhibitor complex [23], darunavir might be more suitable for the treatment of COVID-19.

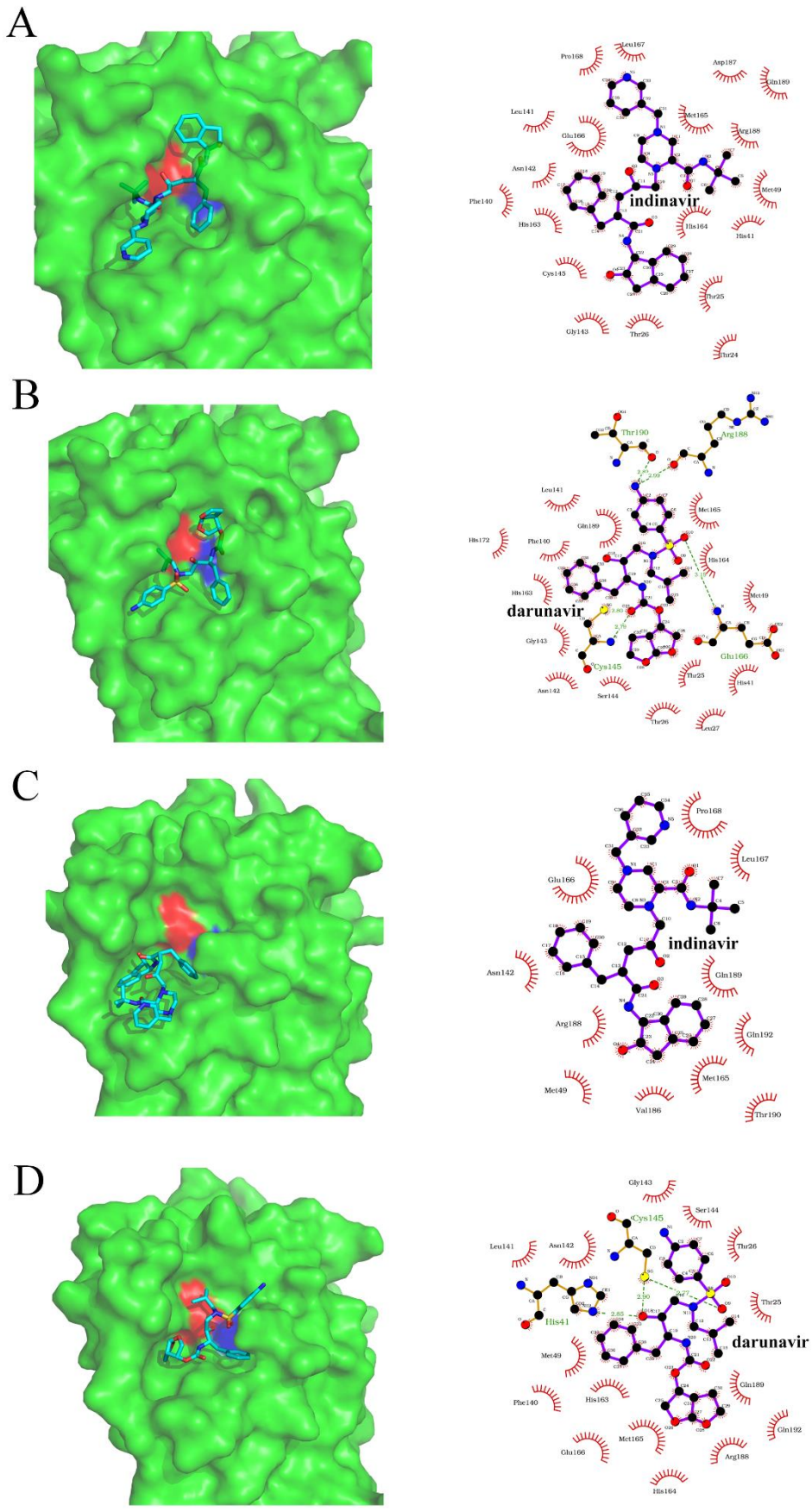

Fig. 4. Predicted binding modes obtained from the docking simulation analyses of indinavir and darunavir toward SARS-CoV-2 and SARS-CoV 3CLpro. Notes: Structures of 3CLpro are shown as molecular surface model in green. The indinavir and darunavir are represented as stick model, and their contact residues in 3CLpro are defined by LigPlot program [24]. The H41 and C145 residues consisting the catalytic dyad are highlighted in red and blue, respectively. The HBs formed between darunavir and 3CLpro residues are labeled in green. (A) SARS-CoV-2 3CLpro-indinavir complex. Indinavir binds deeply into its pocket, makes contact with 19 residues, and forms zero HB with 3CLpro. (B) SARS-CoV-2 3CLpro-darunavir complex. Darunavir binds deeply into its pocket, makes contact with 19 residues, and forms five HBs with 3CLpro. (C) SARS-CoV 3CLpro-indinavir complex. Indinavir binds shallowly to the surface of its pocket, makes contact with 11 residues, and forms zero HB with 3CLpro. (D) SARS-CoV 3CLpro-darunavir complex. Darunavir binds shallowly to the surface of its pocket, makes contact with 17 residues, and forms three HB with 3CLpro.

3.2 Binding free energy calculation

In order to explore the binding mechanism of 3CLpro towards indinavir and darunavir, the docked complex structures, i.e., SARS-CoV-2-indinavir, SARS-CoV-2-darunavir, SARS-CoV-indinavir and SARS-CoV-darunavir, were subjected to 20 ns molecular dynamics simulations. The simulation trajectories were used to calculate the binding free energy by MM-PBSA method. As presented in Table 2, the binding free energy of SARS-CoV-2 3CLpro is about twice as low as that of SARS-CoV for both of indinavir and darunavir, suggesting that these two of inhibitors bind more tightly to the former 3CLpro. Close examination of Table 2 suggests that the primary force driving the binding events for both SARS-CoV-2 and SARS-CoV 3CLpro are the vacuum potential energy (ΔE_{MM}) and nonpolar energies ($\Delta G_{nonpolar}$). In contrast, the polar energies (ΔG_{polar}) negatively contribute to the binding events.

In accordance with the results of molecular docking, the final binding free energy value for darunavir and SARS-CoV-2 3CLpro is lower than that of indinavir (-72.11 kJ/mol for indinavir and -95.53 kJ/mol for darunavir), indicating the higher binding affinity of the former towards 3CLpro than the latter. Detailed decomposition of the several energy components reveals that the decreased binding free energy of darunavir is mainly due to the reduced negative contribution of ΔG_{polar} (173.57 kJ/mol for indinavir and 121.27 kJ/mol for darunavir), although the positive contribution of ΔE_{MM} is even lower than for indinavir (-226.53 kJ/mol for indinavir and -196.94 kJ/mol for darunavir). Taken together, darunavir which could be used as template for structure-based design of SARS-CoV-2 3CLpro inhibitors, has the potential to become an anti-COVID-19 clinical drug.

Table 2. Binding free energy calculated by MM-PBSA method

Energy Components （kJ/mol）	SARS-CoV-2-indinavir	SARS-CoV-2-darunavir	SARS-CoV-indinavir	SARS-CoV-darunavir
ΔE_{ele}	-54.98	-24.23	-5.17	-30.29
ΔE_{vdw}	-171.55	-172.71	-68.23	-138.96
ΔE_{MM}	-226.53	-196.94	-73.4	-169.25
ΔG_{polar}	173.57	121.27	45.8	138.74
$\Delta G_{nonpolar}$	-19.15	-19.86	-9.3	-16.58

ΔG_{sol}	154.42	101.41	36.5	122.16
$\Delta G_{binding}$	-72.11	-95.53	-36.9	-47.09

3.3 Dynamic properties of SARS-CoV-2 and SARS-CoV 3CLpro

In order to investigate the likely reason behind the increased binding affinity of HIV-1 protease inhibitors toward SARS-CoV-2 3CLpro than that of SARS-CoV, 100 ns MD simulations were performed on these two kinds of free enzymes without any inhibitor. Based on the obtained MD trajectories, the root mean square fluctuation (RMSF) for each residue was calculated in order to analyze and compare the structural flexibility of the SARS-CoV-2 and SARS-CoV 3CLpro. The resulting RMSFs are displayed in Fig. 5 as a function of residue number as well as the 3D backbone representations of 3CLpro colored according to the RMSF values. As shown in Fig. 5, the SARS-CoV-2 3CLpro has an overall higher flexibility (or lower rigidity) than that of SARS-CoV 3CLpro in domain I and domain II region. Close examination of Fig. 5 reveals that the SARS-CoV 3CLpro displays lower flexibility in some regions of surface-exposed loops, especially that of substrate binding pocket (Fig. 5B and C). Interestingly, when comparing the domain III region, the SARS-CoV-2 3CLpro is less flexible (i.e. more rigid) than the SARS-CoV 3CLpro. It is well established that flexibility plays significant role in protein function [25]. For example, higher flexibility could enlarge the substrate binding pocket thus increasing the kinetics of substrate entrance and product egress [26]. In addition, the presence of flexibility could also increase the substrate binding affinity [27]. Therefore, a lower flexibility in domain I and domain II regions, especially that of the substrate binding pocket, might explain why the binding affinity of HIV-1 protease inhibitors toward SARS-CoV-2 3CLpro is higher than that of SARS-CoV .

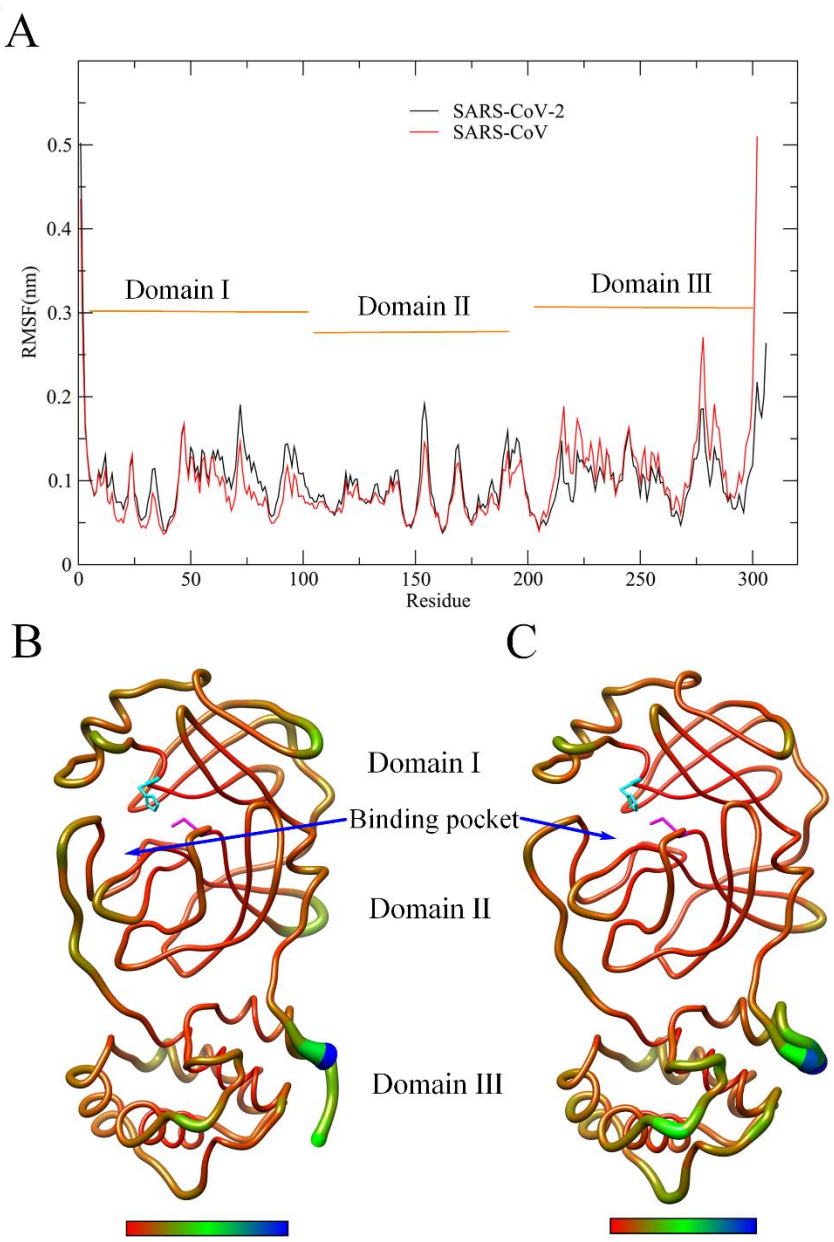

Fig. 5. Comparison between the structural flexibility of SARS-CoV-2 and SARS-CoV 3CLpro. (A) Per-residue average backbone RMSF profiles calculated from MD trajectories of SARS-CoV-2 (black line) and SARS-CoV (red line) 3CLpro. (B) and (C) are 3D backbone representations of SARS-CoV-2 and SARS-CoV 3CLpro structures mapped with per-residue average backbone RMSF values, respectively. The backbone color ranges from red to blue and corresponds to a line from thin to thick, and denotes that the backbone RMSF varies from the lowest to the highest values. The H41 and C145 residues consisting the catalytic dyad are represented in cyan and magenta stick models, respectively. (B) and (C) were generated using UCSF Chimera [28].

4. Conclusion

A novel severe acute respiratory syndrome coronavirus (SARS-CoV-2) was identified from respiratory illness patients in Wuhan, Hubei Province, China, which has recently emerged as a serious threat to the world public health. Hower, no approved drugs have been found to effectively inhibit the virus. Since the urgent of the epidemic situation, it is an effective way to choose the old drugs for clinical treatment. It has been reported that HIV-1 inhibitors can be used as anti-SARS clinical treatment drugs by targeting the SARS-CoV 3CLpro. In this study, we choose six approved anti-HIV-1 inhibitor drugs to evaluate and compare their binding affinity with SARS-CoV-2 and SARS-CoV 3CLpro by molecular docking and MM-PBSA binding free energy calculations. Our results show that darunavir has the best binding affinity with SARS-CoV-2 and SARS-CoV 3CLpro among all inhibitors, indicating it has the potential to become an anti-COVID-19 clinical drug. The likely reason behind the increased binding affinity of HIV-1 protease inhibitors toward SARS-CoV-2 3CLpro than that of SARS-CoV were investigated by MD simulations. The calculated RMSF values for each residue during simulation indicate that the lower flexibility in domain I and domain II regions of SARS-CoV, especially that of the substrate binding pocket, might explain why the binding affinity of HIV-1 protease inhibitors toward SARS-CoV-2 3CLpro is higher than that of SARS-CoV. Our study provides insight into the possible role of structural flexibility during interactions between 3CLpro and inhibitors, and sheds light on the structure-based design of anti-COVID-19 drugs targeting the SARS-CoV-2 3CLpro.

Conflict of interests

The authors declare no conflicts of interest for this work.

Acknowledgments

This study was funded by the National Natural Sciences Foundation of China (31860243 and 31660015) and Yunnan Applied Basic Research Projects (2017FH001-032 and 2017FB024).

References

[1] Zhu N, Zhang D, Wang W, Li X, Yang B, Song J, et al. A novel coronavirus from patients with pneumonia in China, 2019. New England Journal of Medicine. 2020.

[2] Xu X, Chen P, Wang J, Feng J, Zhou H, Li X, et al. Evolution of the novel coronavirus from the ongoing Wuhan outbreak and modeling of its spike protein for risk of human transmission. SCIENCE CHINA Life Sciences. 2020.

[3] Reddy AD, Suh SB, Ghaffari R, Singh NJ, Kim D-J, Han JH, et al. Bioinformatics analysis of SARS proteins and molecular dynamics simulated structure of an alpha-helix motif. BULLETIN-KOREAN CHEMICAL SOCIETY. 2003;24:899-900.

[4] Xia B, Kang X. Activation and maturation of SARS-CoV main protease. Protein & cell. 2011;2:282-90.

[5] Lu I-L, Mahindroo N, Liang P-H, Peng Y-H, Kuo C-J, Tsai K-C, et al. Structure-based drug design and structural biology study of novel nonpeptide inhibitors of severe acute respiratory syndrome coronavirus main protease. Journal of medicinal chemistry. 2006;49:5154-61.

[6] Yang H, Yang M, Ding Y, Liu Y, Lou Z, Zhou Z, et al. The crystal structures of severe acute respiratory syndrome virus main protease and its complex with an inhibitor. Proceedings of the National Academy of Sciences. 2003;100:13190-5.

[7] Báez-Santos YM, John SES, Mesecar AD. The SARS-coronavirus papain-like protease: structure, function and

inhibition by designed antiviral compounds. Antiviral research. 2015;115:21-38.
[8] Lee C-C, Kuo C-J, Hsu M-F, Liang P-H, Fang J-M, Shie J-J, et al. Structural basis of mercury-and zinc-conjugated complexes as SARS-CoV 3C-like protease inhibitors. FEBS letters. 2007;581:5454-8.
[9] Bond CS, Schuttelkopf AW. ALINE: a WYSIWYG protein-sequence alignment editor for publication-quality alignments. Acta crystallographica Section D, Biological crystallography. 2009;65:510-2.
[10] Schrodinger, LLC. The PyMOL Molecular Graphics System, Version 1.8. 2015.
[11] Nukoolkarn V, Lee VS, Malaisree M, Aruksakulwong O, Hannongbua S. Molecular dynamic simulations analysis of ritronavir and lopinavir as SARS-CoV 3CLpro inhibitors. Journal of theoretical biology. 2008;254:861-7.
[12] Zhang XW, Yap YL. Old drugs as lead compounds for a new disease? Binding analysis of SARS coronavirus main proteinase with HIV, psychotic and parasite drugs. Bioorganic & medicinal chemistry. 2004;12:2517-21.
[13] Yamamoto N, Yang R, Yoshinaka Y, Amari S, Nakano T, Cinatl J, et al. HIV protease inhibitor nelfinavir inhibits replication of SARS-associated coronavirus. Biochemical and biophysical research communications. 2004;318:719-25.
[14] Goodsell DS, Morris GM, Olson AJ. Automated docking of flexible ligands: applications of AutoDock. Journal of molecular recognition. 1996;9:1-5.
[15] Hess B, Kutzner C, Van Der Spoel D, Lindahl E. GROMACS 4: algorithms for highly efficient, load-balanced, and scalable molecular simulation. Journal of chemical theory and computation. 2008;4:435-47.
[16] Best RB, Zhu X, Shim J, Lopes PE, Mittal J, Feig M, et al. Optimization of the additive CHARMM all-atom protein force field targeting improved sampling of the backbone φ, ψ and side-chain χ1 and χ2 dihedral angles. Journal of chemical theory and computation. 2012;8:3257-73.
[17] Vanommeslaeghe K, Hatcher E, Acharya C, Kundu S, Zhong S, Shim J, et al. CHARMM general force field: A force field for drug‐like molecules compatible with the CHARMM all‐atom additive biological force fields. Journal of computational chemistry. 2010;31:671-90.
[18] Yu W, He X, Vanommeslaeghe K, MacKerell Jr AD. Extension of the CHARMM general force field to sulfonyl‐containing compounds and its utility in biomolecular simulations. Journal of computational chemistry. 2012;33:2451-68.
[19] Jorgensen WL, Chandrasekhar J, Madura JD, Impey RW, Klein ML. Comparison of simple potential functions for simulating liquid water. The Journal of chemical physics. 1983;79:926-35.
[20] Sang P, Xie Y-H, Li L-H, Ye Y-J, Hu W, Wang J, et al. Effect of the R119G mutation on human P5CR structure and its interactions with NAD: insights derived from molecular dynamics simulation and free energy analysis. Computational biology and chemistry. 2017;67:141-9.
[21] Wang C, Greene DA, Xiao L, Qi R, Luo R. Recent developments and applications of the MMPBSA method. Frontiers in molecular biosciences. 2018;4:87.
[22] Kumari R, Kumar R, Consortium OSDD, Lynn A. g_mmpbsa · A GROMACS tool for high-throughput MM-PBSA calculations. Journal of chemical information and modeling. 2014;54:1951-62.
[23] Du X, Li Y, Xia Y-L, Ai S-M, Liang J, Sang P, et al. Insights into protein–ligand interactions: mechanisms, models, and methods. International journal of molecular sciences. 2016;17:144.
[24] Laskowski RA, Swindells MB. LigPlot+: multiple ligand-protein interaction diagrams for drug discovery. J Chem Inf Model. 2011;51:2778-86.
[25] Kokkinidis M, Glykos N, Fadouloglou V. Protein flexibility and enzymatic catalysis. Adv Protein Chem Struct Biol. 2012;87:181-218.
[26] Chen J, Chen H, Shi Y, Hu F, Lao X, Gao X, et al. Probing the effect of the non-active-site mutation Y229W in New Delhi metallo-β-lactamase-1 by site-directed mutagenesis, kinetic studies, and molecular dynamics

simulations. PLoS One. 2013;8.
[27] Liu S-Q, Tao Y, Meng Z-H, Fu Y-X, Zhang K-Q. The effect of calciums on molecular motions of proteinase K. Journal of molecular modeling. 2011;17:289-300.
[28] Pettersen EF, Goddard TD, Huang CC, Couch GS, Greenblatt DM, Meng EC, et al. UCSF Chimera--a visualization system for exploratory research and analysis. J Comput Chem. 2004;25:1605-12.